

Critical Motility-Induced Phase Separation in Three Dimensions is Consistent with Ising Universality

Jiechao Feng¹ and Ahmad K. Omar^{2,3,*}

¹Graduate Group in Applied Science & Technology, University of California, Berkeley, California 94720, USA

²Department of Materials Science and Engineering, University of California, Berkeley, California 94720, USA

³Materials Sciences Division, Lawrence Berkeley National Laboratory, Berkeley, California 94720, USA

Numerical investigations aiming to determine the universality class of critical motility-induced phase separation (MIPS) in two dimensions (2D) have resulted in inconclusive findings. Here, using finite-size scaling results obtained from large-scale computer simulations, we find that the static and dynamic critical exponents associated with 3D MIPS all closely match those of the 3D Ising universality class with a conserved scalar order parameter. This finding is corroborated by fluctuating hydrodynamic description of the critical dynamics of the order parameter field which precisely matching model B in three dimensions. Our work suggests that 3D MIPS and indeed the entire phase diagram of active Brownian spheres is remarkably similar to that of molecular passive fluids despite the absence of Boltzmann statistics.

Introduction.— In thermodynamic equilibrium, critical points of continuous phase transitions have been understood for over a half century [1–5]. Despite what can appear to be vastly disparate microscopic details, systems with the same symmetries and satisfying the same conservation laws will behave remarkably similar near their respective critical points [4–6]. This behavior includes how the correlation length and response functions diverge (governed by *static* critical exponents) and even how the dynamics slow down (set by *dynamic* exponents [7]) as the critical point is approached. The universality of critical phenomena is not restricted to thermodynamic equilibrium. The study of critical phenomena in intrinsically nonequilibrium systems has revealed novel fixed points that belong to universality classes exclusive to driven [8–12] and/or active [13–19] systems.

The observation of activity-induced phase transitions in recent years has become routine, with many of the transitions exhibiting a critical point. Among the more well-studied active transitions is known as “motility-induced phase separation” (MIPS), the phenomena in which non-aligning and purely repulsive active particles may phase separate into co-existing domains of disordered fluids [20–23]. The similarity of MIPS to a traditional liquid-gas transition (i.e., bulk coexistence solely characterized by a conserved scalar order parameter) is suggestive of Ising universality. Several investigations have sought to numerically determine the universality class of MIPS in two dimensions (2D) using both on- [24, 25] and off-lattice [26, 27] simulations. While the results of some of these studies are indeed consistent with Ising universality [24, 27], others have been less conclusive [25, 26]. In parallel, phenomenological field theories of scalar active matter, including Active Model B+ (AMB+) [28, 29], can, in addition to the Wilson-Fisher fixed point, exhibit a novel fixed point which may be associated with microphase separation [30]. The coalescence of these fixed points in two dimensions can alter the universality class and has been suggested as a possible origin of these conflicting numerical investigations [31].

In this Letter, we aim to shed light on the nature of the MIPS critical point by providing a large-scale numerical in-

vestigation of MIPS in *three dimensions*. Our extensive finite-size scaling analysis results in critical exponents (ν , γ , β , and z) consistent with the 3D Ising universality class with a conserved scalar order parameter. We develop a fluctuating hydrodynamic description of critical MIPS, which can be precisely mapped to model B in three dimensions, suggesting that both the static and dynamic critical exponents should indeed belong to the Ising universality class. We further explore the fluctuating hydrodynamic description of 2D MIPS, finding the presence of marginal terms (in the renormalization group (RG) sense) whose relevance cannot be immediately determined and perhaps is related to the discrepancies in 2D finite-size scaling analyses [24–27]. Our work provides additional evidence that the 3D phase diagram of ABPs is remarkably similar to that of simple substances in thermodynamic equilibrium.

Simulation methods.— We consider the simplest model that captures the critical MIPS behavior: 3D athermal active Brownian hard spheres [32, 33]. Each of the N particles experiences three translational forces: a drag force $-\zeta\dot{\mathbf{x}}$ proportional to the particle velocity $\dot{\mathbf{x}}$ and translational drag coefficient ζ , a conservative interparticle force $\mathbf{F}^C[\mathbf{x}^N]$ where \mathbf{x}^N represents all particle positions, and an active force $\mathbf{F}^A = \zeta U_0 \mathbf{q}$ where U_0 is the intrinsic active speed. Stochastic Brownian translational forces, which simply attenuate the influence of activity, are neglected. The particle orientation \mathbf{q} independently follows diffusive dynamics $\dot{\mathbf{q}} = \boldsymbol{\Omega} \times \mathbf{q}$ where the stochastic angular velocity has mean $\mathbf{0}$ and variance $\langle \boldsymbol{\Omega}(t)\boldsymbol{\Omega}(0) \rangle = 2/\tau_R \delta(t)\mathbf{I}$ and τ_R represents characteristic reorientation time (or inverse rotational diffusion). The interparticle force $\mathbf{F}^C[\mathbf{x}_N; \sigma, \varepsilon]$ is taken from a Weeks-Chandler-Anderson (WCA) potential, which is characterized by a Lennard-Jones diameter σ and energy ε [34]. Taking ζU_0 , σ , and τ_R to be the characteristic units of force, length, and time, respectively, the dimensionless Langevin equation follows as:

$$\ddot{\bar{\mathbf{x}}} = \frac{\ell_0}{\sigma} \left(\mathbf{q} + \bar{\mathbf{F}}^C[\bar{\mathbf{x}}^N; S] \right), \quad (1)$$

where we have defined intrinsic “run length” (activity) $\ell_0 \equiv$

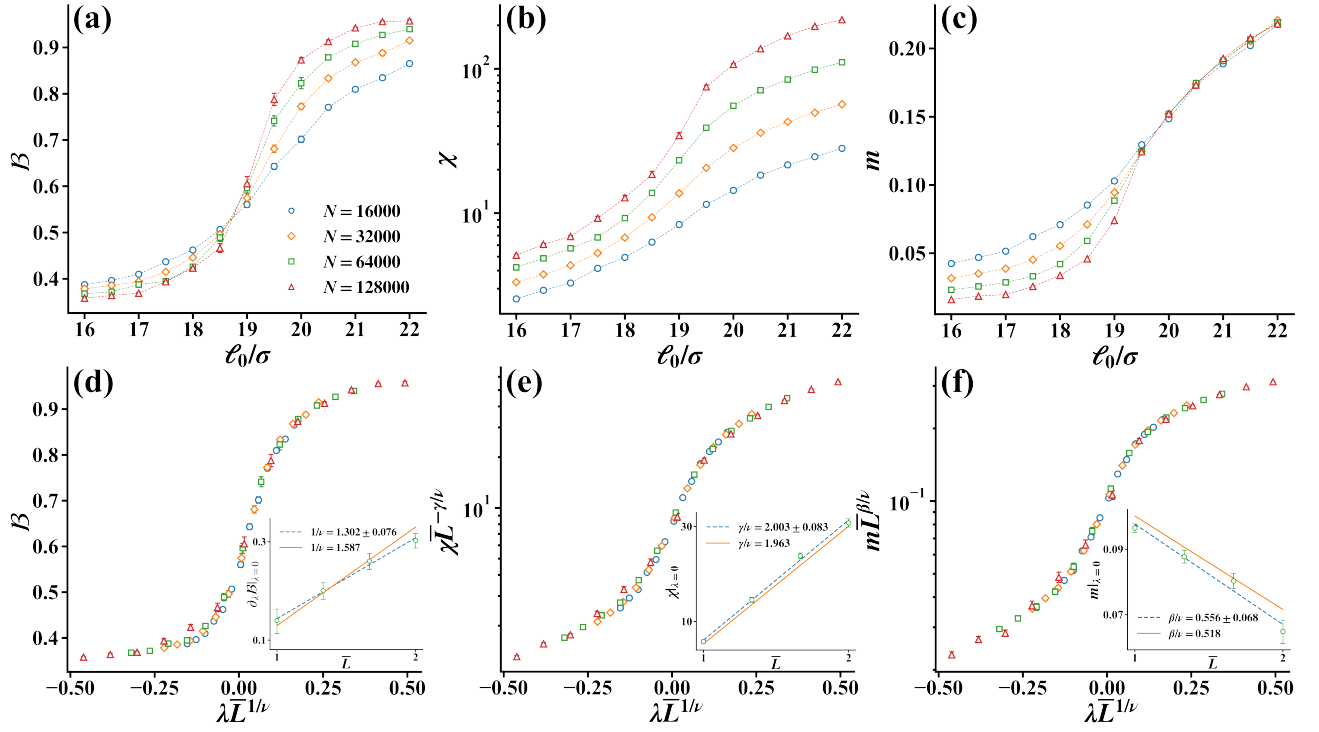


FIG. 1. Finite-size scaling analysis for determining static critical exponents. System size and activity dependence of: (a) B ; (b) χ ; and (c) m . (d) Collapse of data in (a) as a function of the scaling variable $\lambda \bar{L}^{1/\nu}$ with $\nu = 0.630$ (Inset: Slope of B at $\lambda = 0$ ($\ell_0 = \ell_c$) as a function of system size, where the dashed line is the best fit of $1/\nu = 1.302(0.076)$ and the solid line is $1/\nu = 1.587$); (e) collapse of data in (b) with the exponents $\gamma = 1.237$ and $\nu = 0.630$ (Inset: χ at $\lambda = 0$ as a function of system size, where the dashed line is the best fit of $\gamma/\nu = 2.003(0.083)$ and the solid line is $\gamma/\nu = 1.963$); (f) collapse of data in (c) with the exponents $\beta = 0.326$ and $\nu = 0.630$ (Inset: m at $\lambda = 0$ as a function of system size, where the dashed line is the best fit of $\beta/\nu = 0.556(0.068)$ and the solid line is $\beta/\nu = 0.518$). We define $\bar{L} = L/L_0$ where $L_0/\sigma \approx 9.2$ is the size L of the smallest sub-box ($N = 1.6 \times 10^4$).

$U_0\tau_R$. The dimensionless force $\bar{\mathbf{F}}^C$ depends on the reduced positions $\bar{\mathbf{x}}^N$ and is fully characterized by the “stiffness” parameter $\mathcal{S} \equiv \varepsilon/(\zeta U_0\sigma)$. We use $\mathcal{S} = 50$ to effectively achieve hard-sphere statistics. The particles behave precisely as hard spheres in this limit with diameter $d_{\text{hs}} = 2^{1/6}\sigma$, despite the use of a continuous potential. With \mathcal{S} fixed, the system state is fully described by the volume fraction $\phi \equiv Nv_D/V$ and activity ℓ_0/σ , where $v_D \equiv \pi d_{\text{hs}}^3/6$ is the volume of a single particle.

To determine the static critical exponents, we perform simulations with fully periodic boundary conditions using asymmetric boxes with an aspect ratio of 1:1:4 ($L_z = 4L_x = 4L_y$). When above the critical activity, this choice of simulation geometry is found to result in an interface with an average normal direction along the z -dimension (consistent with area-minimizing interfaces [35]). We consider systems of sizes $N = (1.6, 3.2, 6.4, 12.8) \times 10^4$ and examine the statistics of volume fraction fluctuations within subsystems [36–40]. To avoid spurious effects due to the presence of an interface [24–27], we compute the quantities of interest only in four cubic sub-boxes of size $L = L_x/2$ in each of the centers of the dense (liquid) and dilute (gas) phases, allowing us to avoid the interface. All simulations are performed at a fixed overall volume fraction of $\phi = 0.48$, the estimated critical density [32, 41]. All

simulations were conducted using HOOMD-blue [42]. Additional simulation details can be found in the Supplemental Material (SM) [43].

Static critical exponents.— As the critical activity, ℓ_c , is approached the correlation length associated with the order parameter diverges as $\xi \sim \xi_{\pm}|\lambda|^{-\nu}$ where we have defined the reduced activity $\lambda \equiv (\ell_0 - \ell_c)/\ell_c$. The \pm subscript denotes a distinction in properties/functions depending on if λ is greater than or less than zero. We consider observables, \mathcal{O} , that are expected to diverge (or vanish) at the critical point in the absence of finite-size effects. The finite-size scaling ansatz posits the form of these observables, to leading order, as $\mathcal{O} = |\lambda|^{-\zeta_{\mathcal{O}}} F_{\mathcal{O}_{\pm}}(\xi/L)$ where $\zeta_{\mathcal{O}}$ and $F_{\mathcal{O}_{\pm}}$ are the associated critical exponent and scaling functions. Finite system sizes prevent these observables from truly diverging at the critical point and, for $\xi \gg L$, we thus expect $\mathcal{O} = L^{\zeta_{\mathcal{O}}/\nu} \bar{F}_{\mathcal{O}_{\pm}}(|\lambda|(L/\xi_{\pm})^{1/\nu})$ [5]. This implies that all values of \mathcal{O} measured for different system sizes should collapse when $\mathcal{O}L^{-\zeta_{\mathcal{O}}/\nu}$ is plotted as a function of $\lambda L^{1/\nu}$ and should scale as $L^{\zeta_{\mathcal{O}}/\nu}$ precisely at $\ell_0 = \ell_c$. We consider three observables which are related to the statistics of volume fraction fluctuations within sub-boxes. The first is the fourth-order (Binder) cumulant defined as $B \equiv \langle \Delta\phi^2 \rangle_L^2 / \langle \Delta\phi^4 \rangle_L$, where $\Delta\phi = \phi - \langle \phi \rangle_L$, $\langle \phi \rangle_L$ is the average volume fraction

of all sub-boxes, and $\langle \dots \rangle_L$ indicates an average over configurations and all sub-boxes. The second is the susceptibility, $\chi \equiv (L^3/v_D)\langle \Delta\phi^2 \rangle_L / \langle \phi \rangle_L$, which is proportional to the variance of volume fraction fluctuations (again, the expectation is using the distribution computed over all sub-boxes). The final observable we consider is the difference between the average volume fraction of the two phases defined as $m \equiv \langle \phi \rangle_{L,l} - \langle \phi \rangle_{L,g}$, where $\langle \dots \rangle_{L,l}$ and $\langle \dots \rangle_{L,g}$ denote the average over liquid and gas sub-boxes, respectively. The scaling exponents (i.e., $\zeta_{\mathcal{O}}$) for our three observables of \mathcal{B} , χ , m are 0, γ , $-\beta$, respectively.

The Binder cumulant (straightforwardly related to the Binder parameter [36]) allows us to identify the location of the critical point as \mathcal{B} is size-independent at $\ell_0 = \ell_c$. Figure 1(a) displays the activity dependence of \mathcal{B} for several system sizes with all curves intersecting between $18.5 < \ell_c/\sigma < 19.0$, an uncertainty that is appreciably smaller than in previous 2D simulations [26, 27]. The critical activity is estimated to be $\ell_c/\sigma = 18.85(0.05)$ using the two largest system sizes. Using this value and the 3D Ising exponent $\nu = 0.630$ [44], all \mathcal{B} curves nicely collapse onto a universal curve [see Fig. 1(d)]. We also extract the exponent ν from the derivative of \mathcal{B} at criticality: $d\mathcal{B}/d\lambda|_{\lambda=0} \propto L^{1/\nu}$. Importantly, differentiating \mathcal{B} near the critical point likely leads to considerable error. Indeed, we find $\nu = 0.768(0.045)$, a marked deviation from the value for Ising universality. Our measured discrepancy of ν between simulations and the Ising value is smaller than that measured in Siebert *et al.*'s 2D simulations [26] but larger than that reported by Maggi *et al.* [27]. Below, we offer an alternative measure for determining ν that avoids differentiation and results in an exponent that is much more consistent with Ising universality.

We next study the scaling of susceptibility χ . The raw data and the scaled results of χ are shown respectively in Fig. 1(b) and (e). We again find that 3D Ising exponents (now introducing $\gamma = 1.237$ [44]) lead to good collapse. At criticality, we expect $\chi|_{\lambda=0} \propto L^{\gamma/\nu}$. Using this relation, we extract $\gamma/\nu = 2.003(0.083)$, which is in excellent agreement with the 3D Ising value and well within our statistical uncertainty. We note that in previous simulation studies of MIPS critical scaling, this is generally the exponent with the smallest discrepancy from the Ising value [24–27].

Finally, we determine β from the scaling of the phase volume fraction difference, m . Figure 1(c) shows the raw data, where we see immediately that m becomes size-independent above the critical point. Figure 1(f) again shows good data collapse using the 3D Ising exponents including $\beta = 0.326$ [44]. At criticality, we expect $m \propto L^{-\beta/\nu}$, from which we extract $\beta/\nu = 0.556(0.068)$, which is close to the Ising value. We can also obtain the exponent β from $m \propto \lambda^\beta$ for $\lambda \gtrsim 0$, finding $\beta = 0.347(0.008)$ for the largest system, which is again relatively close to the Ising value [43]. From our extracted value of β/ν and β , we estimate $\nu = 0.624(0.078)$, which is nearly exactly the Ising value (in contrast to our earlier estimate using $d\mathcal{B}/d\lambda|_{\lambda=0}$). We note that for 2D MIPS, β appears to be the most controversial exponent: Ref. [26]

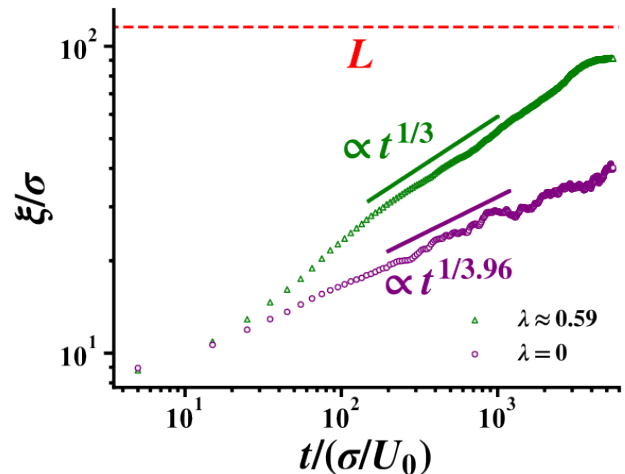


FIG. 2. The correlation length $\xi(t)$ at criticality ($\lambda = 0$, purple circles) and inside phase-separation regime ($\lambda \approx 0.59$, green triangles), as determined from the inverse of the first moment of the static structure factor. Each point represents the average of ten consecutive data points, computed at intervals of σ/U_0 . The purple line shows $t^{1/z}$, where $z = 4 - \eta \approx 3.964$ for model B in 3D. The green line shows $t^{1/3}$ which is the classical scaling for Ostwald ripening and/or coalescence. The red dashed line denotes the upper limit for ξ , which is the system size L .

found β is appreciably larger than the 2D Ising value, while the on-lattice simulation in Ref. [25] also showed large discrepancies of both β and β/ν with Ising values. The relatively small discrepancies between all of our measured exponents and Ising exponents in comparison to 2D studies may point towards a genuine distinction between 2D and 3D MIPS. We will later discuss the possible origins of this dimensionality dependence.

Dynamic critical exponent.— While the static exponents of 3D MIPS are consistent with Ising universality, systems sharing the same static critical exponents can exhibit different dynamic exponents, depending on their equations of motion. This raises the question of whether activity could manifest through a modification of the critical dynamics. Approaching the critical point, as the correlation length diverges, one expects the associated dynamical relaxation time to grow as well with $\tau \sim \xi^z$ where we have defined the dynamic critical exponent z [3, 5]. Here, τ is the relaxation time of spatial correlations of the order parameter on length scales of ξ . For finite system sizes, the time evolution of the correlation length as it approaches its steady state value offers insight into this dynamic exponent. Dimensional analysis suggests the following $\xi(t) = \xi(t \rightarrow \infty) \mathcal{F}_t(t/\tau)$ where \mathcal{F}_t is a scaling function and we have assumed an initial condition of a random quench with a small correlation length. This scaling hypothesis is thus only anticipated to hold beyond some initial duration after the quench, τ_0 . Near the critical point, the finite system size bounds the terminal correlation length with $\xi(t \rightarrow \infty) = L$ and thus also bounds the relaxation time to $\tau \sim L^z$. Prior to reaching this terminal value the correlation length follows

$\xi(t) = L\mathcal{F}_t(t/\tau)$. For $t \ll \tau$ (while $t > \tau_0$) the time-dependent correlation length should be independent of the system size. In this regime, a power-law expansion of the scaling function must take the form $\mathcal{F}_t(t/\tau) \sim (t/\tau)^{1/z}$ to ensure the independence of $\xi(t)$ with the system size. We therefore anticipate a window of time ($\tau_0 < t \ll \tau$) in which $\xi(t) \sim t^{1/z}$. In the case of model B dynamics, the longest relaxation time is set by the diffusive motion with $\tau \sim \xi^2/D$. This diffusivity is the collective (or chemical) diffusivity that, in the case of a single conserved scalar order parameter, can be expressed as the product of an Onsager transport coefficient, M , and the inverse susceptibility with $D \sim M/\chi$. If we assume that the Onsager mobility displays no singular behavior as the critical point is approached, we then have $\tau \sim \xi^2\chi \sim \xi^{2+\gamma/\nu}$ and the critical exponent is entirely determined from the static exponents with $z = 2 + \gamma/\nu \equiv 4 - \eta$ ($z \approx 3.964$ or $\eta \approx 0.036$ for 3D Ising universality with conserved dynamics). We note that previous studies on 2D MIPS have found the critical dynamics of MIPS belong to the 2D Ising universality class with conserved dynamics ($\eta = 1/4$ [24, 45]) but, to the best of our knowledge, z has not been determined for critical 3D MIPS.

To numerically determine z for critical MIPS, we first need to define the correlation length from simulations. We follow previous works [46–49] and determine the correlation length $\xi(t)$ from the inverse of the first moment of the static structure factor [43]. Figure 2 presents the time-dependence of this length scale after a quench to the critical point ($\lambda = 0$) for our largest system size $N = 10^6$. While no power-law scaling is observed at early or late times (as anticipated), we do find an intermediate time window in which the correlation length scales with time in agreement with 3D Ising universality under model B dynamics, characterized by $z \approx 3.96$ (see SM for detailed analysis [43]). This behavior is contrasted with a deep quench ($\lambda \approx 0.59$ in Fig. 2) which reveals a scaling exponent of $1/3$, consistent with classical theories of Ostwald ripening and/or coalescence [47, 50–52]. It thus appears that both the static and dynamic exponents of critical 3D MIPS are entirely consistent with those of 3D Ising universality class.

Coarse-grained dynamics.— The consistency of our numerical results with 3D Ising universality motivates a reexamination of the fluctuating hydrodynamic equations of active Brownian spheres. These fluctuating hydrodynamics were developed recently through the systematic coarse-graining of the equation of motion corresponding to Eq. (1) (see Ref. [35] and End Matter for details). To obtain a hydrodynamic description that solely contains the density field, closures and controlled approximations are introduced that limit the applicability of the theory to systems with repulsive interactions, finite activity, small density gradients (large wavelength and small amplitude), and long times. We expect that near-critical dynamics are within these limits.

Our fluctuating hydrodynamic theory identifies that local density $\rho(\mathbf{r}, t)$ evolution is driven by gradients in stress and a stochastic athermal noise term. The noise statistics, while approximate for the coarse-grained fields of interest, contains an off-diagonal term which can be expressed in terms of density

gradients. The coarse-grained description is then expanded around the critical point, and motivates the introduction of a shifted order parameter field, $\varphi(\mathbf{r}, t) \equiv \rho(\mathbf{r}, t) - \rho_c$. The expression of stresses now includes a bulk pressure which can be written as a power series of φ and gradient terms. The critical density ρ_c and activity ℓ_c are determined by the vanishing of the first two derivatives of the bulk term of stresses. More details can be found in the End Matter.

To analyze the critical fluctuations, we first determine the Janssen-De Dominicis action governing the dynamics [5]. In this approach, an auxiliary field enforces our equation of motion. We next conduct a standard dimensional analysis to determine the relevance of different terms in the RG sense. We enforce that the action itself is scale invariant and determine the flow equations for the coefficients appearing in the action. In $d = 3$, higher-order gradient contributions like $|\nabla\varphi|^2$ are irrelevant, and the noise near criticality is effectively Gaussian. This reduction yields an action consistent with model B dynamics:

$$\frac{\partial\varphi}{\partial t} = \frac{1}{\zeta}\nabla^2 \left((g_1 - a\nabla^2)\varphi + g_2\varphi^2 + g_3\varphi^3 + \text{h.o.t.} \right) + \nabla \cdot \boldsymbol{\eta}, \quad (2a)$$

$$\langle \boldsymbol{\eta}(\mathbf{r}, t) \boldsymbol{\eta}(\mathbf{r}', t') \rangle = 2 \frac{k_B T^{\text{act}}}{\zeta} \rho_c \mathbf{I} \delta(t - t') \delta(\mathbf{r} - \mathbf{r}'), \quad (2b)$$

where a, g_1, g_2, g_3, \dots are expansion coefficients, $k_B T^{\text{act}} \equiv \zeta U_0 \ell_0 / d(d-1)$ is the active energy scale, and h.o.t. indicates higher-order terms which are irrelevant. At the critical point, $g_1 = g_2 = 0$ so that the Wilson-Fisher fixed point governs the dynamics, consistent with the Ising universality class for both the static and dynamic exponents with a conserved scalar order parameter.

The theory is less conclusive in two dimensions. With $d = 2$, the field φ becomes dimensionless, and all coupling terms from the power-series expansion of φ are equally relevant. Moreover, higher-order gradient terms like $|\nabla\varphi|^2$ and the multiplicative noise term become marginal, so that one cannot readily recover the effective model B dynamics. These marginal terms may underlie the contradictory simulation results for the universality class of 2D MIPS [24–27]. Notably, the inconclusive results in two dimensions may possibly result from the additional fixed points found in the phenomenological AMB+ [28, 29] that coincide with the Wilson-Fisher fixed point in the limit $d \rightarrow 2$ [30]. Although these fixed points have not been formally established in microscopic models (e.g., ABPs), some phenomenology—such as microphases [29, 47, 53–55]—is superficially consistent with their predictions. In three-dimensional particle-based simulations, there is no evidence that these exotic fixed points found in AMB+ arise; we find only standard bulk phase separation consistent with Ising universality. Further studies are needed to ascertain whether marginal terms or additional ordering fields can destabilize the Wilson-Fisher fixed point in two dimensions, and such investigations are central to reconciling conflicting simulation results and fully understanding the nature of critical MIPS.

Conclusions.— We have presented extensive simulations to extract critical exponents ν , γ , β , and z of 3D MIPS, all of which closely match those of the 3D Ising universality class with conserved dynamics. Theoretically, our fluctuating hydrodynamic description of the order parameter field expanded about the critical point also matches that of model B in 3D but our analysis is inconclusive in 2D. These findings lead us to conclude that MIPS in 3D belongs to Ising universality class, while the entire phase diagram of ABPs remarkably resembles that of passive fluids with attractive interactions [32, 56]: a critical point with Ising universality, a triple point, and a largely metastable liquid-gas transition. Active Brownian particles are thus able to entirely reproduce the classical phase diagram of passive molecular systems despite breaking time-reversal symmetry.

J.F. acknowledges support from the UC Berkeley College of Engineering Jane Lewis Fellowship. This research used the Savio computational cluster resource provided by the Berkeley Research Computing program.

* aomar@berkeley.edu

- [1] L. P. Kadanoff, W. Götzke, D. Hamblen, R. Hecht, E. A. S. Lewis, V. V. Palciauskas, M. Rayl, J. Swift, D. Aspnes, and J. Kane, *Rev. Mod. Phys.* **39**, 395 (1967).
- [2] M. E. Fisher, *J. Math. Phys.* **5**, 944 (1964).
- [3] P. C. Hohenberg and B. I. Halperin, *Rev. Mod. Phys.* **49**, 435 (1977).
- [4] M. Kardar, *Statistical physics of fields* (Cambridge University Press, 2007).
- [5] U. C. Täuber, *Critical dynamics: a field theory approach to equilibrium and non-equilibrium scaling behavior* (Cambridge University Press, 2014).
- [6] H. E. Stanley, *Rev. Mod. Phys.* **71**, S358 (1999).
- [7] G. Ódor, *Rev. Mod. Phys.* **76**, 663 (2004).
- [8] S. Katz, J. L. Lebowitz, and H. Spohn, *Phys. Rev. B* **28**, 1655 (1983).
- [9] M. Kardar, G. Parisi, and Y.-C. Zhang, *Phys. Rev. Lett.* **56**, 889 (1986).
- [10] J. Cardy and U. C. Täuber, *Phys. Rev. Lett.* **77**, 4780 (1996).
- [11] I. Dornic, H. Chaté, J. Chave, and H. Hinrichsen, *Phys. Rev. Lett.* **87**, 45701 (2001).
- [12] K. A. Takeuchi, M. Kuroda, H. Chaté, and M. Sano, *Phys. Rev. Lett.* **99**, 234503 (2007).
- [13] J. Toner and Y. Tu, *Phys. Rev. Lett.* **75**, 4326 (1995).
- [14] J. Toner and Y. Tu, *Phys. Rev. E* **58**, 4828 (1998).
- [15] J. Toner, *Phys. Rev. E* **86**, 31918 (2012).
- [16] R. Alert, J.-F. Joanny, and J. Casademunt, *Nat. Phys.* **16**, 682 (2020).
- [17] F. Cagnetta, V. Škultéty, M. R. Evans, and D. Marenduzzo, *Phys. Rev. E* **105**, 14610 (2022).
- [18] P. Jentsch and C. F. Lee, *Phys. Rev. Lett.* **133**, 128301 (2024).
- [19] M. Miller and J. Toner, *Phys. Rev. E* **110**, 54607 (2024).
- [20] Y. Fily and M. C. Marchetti, *Phys. Rev. Lett.* **108**, 235702 (2012).
- [21] G. S. Redner, M. F. Hagan, and A. Baskaran, *Phys. Rev. Lett.* **110**, 55701 (2013).
- [22] I. Buttinoni, J. Bialké, F. Kümmel, H. Löwen, C. Bechinger, and T. Speck, *Phys. Rev. Lett.* **110**, 238301 (2013).
- [23] M. E. Cates and J. Tailleur, *Annu. Rev. Condens. Matter Phys.* **6**, 219 (2015).
- [24] B. Partridge and C. F. Lee, *Phys. Rev. Lett.* **123**, 68002 (2019).
- [25] F. Dittrich, T. Speck, and P. Virnau, *Eur. Phys. J. E* **44**, 1 (2021).
- [26] J. T. Siebert, F. Dittrich, F. Schmid, K. Binder, T. Speck, and P. Virnau, *Phys. Rev. E* **98**, 30601 (2018).
- [27] C. Maggi, M. Paoluzzi, A. Crisanti, E. Zaccarelli, and N. Gnan, *Soft Matter* **17**, 3807 (2021).
- [28] C. Nardini, É. Fodor, E. Tjhung, F. van Wijland, J. Tailleur, and M. E. Cates, *Phys. Rev. X* **7**, 21007 (2017).
- [29] E. Tjhung, C. Nardini, and M. E. Cates, *Phys. Rev. X* **8**, 31800 (2018).
- [30] F. Caballero, C. Nardini, and M. E. Cates, *J. Stat. Mech.* **2018**, 123208 (2018).
- [31] T. Speck, *Phys. Rev. E* **105**, 64601 (2022).
- [32] A. K. Omar, K. Klymko, T. GrandPre, and P. L. Geissler, *Phys. Rev. Lett.* **126**, 188002 (2021).
- [33] J. Feng and A. K. Omar, [arXiv:2407.08676](https://arxiv.org/abs/2407.08676) (2024).
- [34] J. D. Weeks, D. Chandler, and H. C. Andersen, *J. Chem. Phys.* **54**, 5237 (1971).
- [35] L. Langford and A. K. Omar, *Phys. Rev. E* **110**, 54604 (2024).
- [36] K. Binder, *Z. Phys. B Condens. Matter* **43**, 119 (1981).
- [37] K. Binder, *Ferroelectrics* **73**, 43 (1987).
- [38] M. Rovere, D. W. Hermann, and K. Binder, *Europhys. Lett.* **6**, 585 (1988).
- [39] M. Rovere, D. W. Heermann, and K. Binder, *J. Phys. Condens. Matter* **2**, 7009 (1990).
- [40] M. Rovere, P. Nielaba, and K. Binder, *Z. Phys. B Condens. Matter* **90**, 215 (1993).
- [41] A. K. Omar, H. Row, S. A. Mallory, and J. F. Brady, *Proc. Nat. Acad. Sci. U.S.A.* **120**, e2219900120 (2023).
- [42] J. A. Anderson, J. Glaser, and S. C. Glotzer, *Comput. Mater. Sci.* **173**, 109363 (2020).
- [43] See Supplemental Material at [URL], which includes Refs. [57–64], for theory of critical fluctuating hydrodynamics for ABPs, numerical details of finite-size scaling analysis, and numerical determination of critical exponents.
- [44] M. Hasenbusch, K. Pinn, and S. Vinti, *Phys. Rev. B* **59**, 11471 (1999).
- [45] F. Dittrich, J. Midya, P. Virnau, and S. K. Das, *Phys. Rev. E* **108**, 24609 (2023).
- [46] J. Stenhammar, A. Tiribocchi, R. J. Allen, D. Marenduzzo, and M. E. Cates, *Phys. Rev. Lett.* **111**, 145702 (2013).
- [47] J. Stenhammar, D. Marenduzzo, R. J. Allen, and M. E. Cates, *Soft Matter* **10**, 1489 (2014).
- [48] R. Wittkowski, A. Tiribocchi, J. Stenhammar, R. J. Allen, D. Marenduzzo, and M. E. Cates, *Nat. Commun.* **5**, 4351 (2014).
- [49] S. Mandal, B. Liebchen, and H. Löwen, *Phys. Rev. Lett.* **123**, 228001 (2019).
- [50] P. M. Chaikin, T. C. Lubensky, and T. A. Witten, *Principles of condensed matter physics*, Vol. 10 (Cambridge university press Cambridge, 1995).
- [51] A. J. Bray, *Adv. Phys.* **51**, 481 (2002).
- [52] S. Puri, *Phase Transitions* **77**, 407 (2004).
- [53] C. B. Caporusso, P. Digregorio, D. Levis, L. F. Cugliandolo, and G. Gonnella, *Phys. Rev. Lett.* **125**, 178004 (2020).
- [54] X.-q. Shi, G. Fausti, H. Chaté, C. Nardini, and A. Solon, *Phys. Rev. Lett.* **125**, 168001 (2020).
- [55] V. Semwal, J. Joshi, S. Dikshit, and S. Mishra, *Physica A* **634**, 129435 (2024).
- [56] D. Evans and A. K. Omar, [arXiv:2411.14536](https://arxiv.org/abs/2411.14536) (2024).
- [57] E. Brézin, D. J. Amit, and J. Zinn-Justin, *Phys. Rev. Lett.* **32**, 151 (1974).

- [58] F. Family, *Physica A* **168**, 561 (1990).
 [59] F. L. Román, J. A. White, and S. Velasco, *J. Chem. Phys.* **107**, 4635 (1997).
 [60] J. M. López, M. A. Rodríguez, and R. Cuerno, *Phys. Rev. E* **56**, 3993 (1997).
 [61] M. Lässig, *Phys. Rev. Lett.* **80**, 2366 (1998).
 [62] F. L. Román, J. A. White, and S. Velasco, *Europhys. Lett.* **42**, 371 (1998).
 [63] L. D. Landau and E. M. Lifshitz, *Statistical Physics: Volume 5* (Elsevier, 2013).
 [64] P. Virtanen, R. Gommers, T. E. Oliphant, M. Haberland, T. Reddy, D. Cournapeau, E. Burovski, P. Peterson, W. Weckesser, and J. Bright, *Nat. Methods* **17**, 261 (2020).
 [65] Y.-J. Chiu, D. Evans, and A. K. Omar, *arXiv:2409.07620* (2024).
 [66] C. Vause and J. Sak, *Phys. Rev. A* **21**, 2099 (1980).
 [67] J. F. Nicoll and R. K. P. Zia, *Phys. Rev. B* **23**, 6157 (1981).
 [68] O. T. Valls and J. A. Hertz, *Phys. Rev. B* **18**, 2367 (1978).
 [69] Y. C. Kim, M. E. Fisher, and G. Orkoulas, *Phys. Rev. E* **67**, 61506 (2003).
 [70] M. Yarmolinsky and A. Kuklov, *Phys. Rev. E* **96**, 62124 (2017).
 [71] L. Canet, H. Chaté, B. Delamotte, and N. Wschebor, *Phys. Rev. Lett.* **104**, 150601 (2010).
 [72] P. Digregorio, D. Levis, A. Suma, L. F. Cugliandolo, G. Gonnella, and I. Pagonabarraga, *Phys. Rev. Lett.* **121**, 98003 (2018).
 [73] J. U. Klamser, S. C. Kapfer, and W. Krauth, *Nat. Commun.* **9**, 5045 (2018).

END MATTER

Here we provide detailed arguments on how our coarse-grained dynamics are mapped to model B. The dynamics of the order parameter can be obtained exactly from systematic coarse-graining. These exact dynamics for a specific field are, for all but the simplest cases, coupled to additional fields. However, in certain limits, it may be possible to formally approximate these dynamics through closures that reduce the number of fields. The resulting dynamics can perhaps be connected to phenomenological dynamical descriptions. Beginning from the Toner-Tu model, Partridge and Lee recently used symmetry considerations to describe the density field dynamics of non-aligning active matter [24]. These arguments resulted in a straightforward identification that these critical active dynamics are precisely those of model B and are thus consistent with the Ising universality class.

We recently derived an *approximate* fluctuating hydrodynamic description of overdamped ABPs [35] under the conditions of small fluxes, small spatial gradients, and long times. Under these conditions, the dynamics for the density field are solely in terms of the local density:

$$\frac{\partial \rho}{\partial t} = -\nabla \cdot \mathbf{J}, \quad (3a)$$

$$\mathbf{J} = \frac{1}{\zeta} \nabla \cdot (\boldsymbol{\sigma}^C + \boldsymbol{\sigma}^{\text{act}}) + \boldsymbol{\eta}^{\text{act}}, \quad (3b)$$

$$\boldsymbol{\sigma}^C = [-p_C(\rho) + \kappa_1(\rho)\nabla^2\rho + \kappa_2(\rho)|\nabla\rho|^2] \mathbf{I} + \kappa_3(\rho)\nabla\rho\nabla\rho + \kappa_4(\rho)\nabla\nabla\rho, \quad (3c)$$

$$\boldsymbol{\sigma}^{\text{act}} = [-p_{\text{act}}(\rho) + a(\rho)\nabla^2\rho] \mathbf{I} + b(\rho)\nabla\rho\nabla\rho, \quad (3d)$$

$$\langle \boldsymbol{\eta}^{\text{act}}(\mathbf{r}, t) \boldsymbol{\eta}^{\text{act}}(\mathbf{r}', t') \rangle = 2 \frac{k_B T^{\text{act}}}{\zeta} \left(\rho \mathbf{I} - \frac{d}{d-1} \mathbf{Q}' \right) \times \delta(t-t') \delta(\mathbf{r}-\mathbf{r}'), \quad (3e)$$

$$\mathbf{Q}' = \frac{\rho U_0}{d p_{\text{act}}} (-a(\rho)\nabla^2\rho \mathbf{I} - b(\rho)\nabla\rho\nabla\rho). \quad (3f)$$

In Eq. (3), $\rho(\mathbf{r}, t)$ is the coarse-grained density field, \mathbf{J} the density flux, ζ the single particle translational drag coefficient, $\boldsymbol{\sigma}^C$ the interparticle conservative stress, $\boldsymbol{\sigma}^{\text{act}}$ the active effective stress, $\boldsymbol{\eta}^{\text{act}}$ the athermal stochastic contribution to density flux, \mathbf{Q}' the traceless nematic order density, and d the number of spatial dimensions. The anisotropic noise presented above is entirely athermal with the amplitude set by the active energy scale $k_B T^{\text{act}} \equiv \zeta U_0 \ell_0 / d(d-1)$. The form of the noise presented in Eq. (3e) is exact for the *microscopic* density and nematic field and approximate for the *coarse-grained* fields of interest. $\boldsymbol{\sigma}^C$ [Eq. (3c)] and $\boldsymbol{\sigma}^{\text{act}}$ [Eq. (3d)] are expanded into bulk terms (p_C and p_{act} respectively) and density gradients up to the second order, with $\{\kappa_i(\rho)\}$, $a(\rho)$, and $b(\rho)$ expansion coefficients. As Ref. [41] considered *repulsive* ABPs at high activities, the interfacial coefficients associated with the interaction stress ($\{\kappa_i(\rho)\}$) were discarded as they fundamentally scale with the particle size (σ) while those associated with the active stress [$a(\rho)$ and $b(\rho)$] scale with the run length (ℓ_0). The forms of $\{\kappa_i(\rho)\}$ can be found for pairwise interacting

systems by formally expanding the spatial kernel of the interaction stress (see, for example, Ref. [65]).

We now proceed to expand Eq. (3) about the critical point. We introduce the order parameter $\varphi(\mathbf{r}, t) = \rho(\mathbf{r}, t) - \rho_c$, where ρ_c is the critical density. Defining the dynamic pressure $\mathcal{P}(\rho) = p_C(\rho) + p_{\text{act}}(\rho)$, the critical point can be determined from the following equations [41]:

$$\left. \frac{\partial \mathcal{P}}{\partial \rho} \right|_{\rho_c, \ell_c} = \left. \frac{\partial^2 \mathcal{P}}{\partial \rho^2} \right|_{\rho_c, \ell_c} = 0. \quad (4)$$

As the system approaches the critical point, Eq. (3) can be

expanded around the critical density. This expansion yields the dynamics for the order parameter, $\varphi(\mathbf{r}, t)$. For the bulk term $\mathcal{P}(\rho)$ in Eq. (3), we can Taylor expand it near ρ_c :

$$\begin{aligned} \mathcal{P}(\rho) = & \mathcal{P}_c + g_1 \varphi(\mathbf{r}, t) + g_2 \varphi^2(\mathbf{r}, t) + g_3 \varphi^3(\mathbf{r}, t) \\ & + g_4 \varphi^4(\mathbf{r}, t) + g_5 \varphi^5(\mathbf{r}, t) + \dots \end{aligned} \quad (5)$$

The gradient terms in Eq. (3) can be written as functions of the order parameter near the critical point, e.g. $\{\kappa_i(\rho)\} \rightarrow \{\kappa_i(\varphi)\}$, $\nabla \rho \rightarrow \nabla \varphi$.

Next we conduct a standard dimensional analysis to determine the relevance of different terms. Introducing the Martin-Siggia-Rose auxiliary field $\tilde{\varphi}$, we can express the Janssen-De Dominicis action governing the system dynamics [5]:

$$\mathcal{A}[\tilde{\varphi}, \varphi] = \mathcal{A}_0[\tilde{\varphi}, \varphi] + \mathcal{A}_{\text{noise}}[\tilde{\varphi}, \varphi], \quad (6a)$$

$$\begin{aligned} \mathcal{A}_0[\tilde{\varphi}, \varphi] = & \int d^d r \int dt \left\{ \tilde{\varphi} \frac{\partial \varphi}{\partial t} + \tilde{\varphi} \frac{1}{\zeta} \nabla \cdot \nabla \cdot \left(\left[-g_1 \varphi - g_2 \varphi^2 - g_3 \varphi^3 + \kappa_1 \nabla^2 \varphi + \kappa_2 |\nabla \varphi|^2 + a \nabla^2 \varphi \right] \mathbf{I} \right. \right. \\ & \left. \left. + \kappa_3 \nabla \varphi \nabla \varphi + \kappa_4 \nabla \nabla \varphi + b \nabla \varphi \nabla \varphi + \text{h.o.t.} \right) \right\}, \end{aligned} \quad (6b)$$

$$\mathcal{A}_{\text{noise}}[\tilde{\varphi}, \varphi] = \int d^d r \int dt \left\{ \tilde{\varphi} \nabla \cdot \nabla \cdot \left[\frac{k_B T^{\text{act}}}{\zeta} \left(\rho \mathbf{I} - \frac{d}{d-1} \mathbf{Q}' \right) \tilde{\varphi} \right] \right\}. \quad (6c)$$

Now we are prepared to derive the scaling dimensions of various quantities from Eq. (6). In terms of an arbitrary momentum scale μ , we have the following scaling dimensions as our starting point:

$$[\mathcal{A}] = \mu^0, \quad [r] = \mu^{-1}. \quad (7)$$

We then assume that a and κ_1 are kept fixed under the RG flow (i.e., $[a] = [\kappa_1] = \mu^0$) such that when all $g_i = 0$ ($i = 1, 2, 3, \dots$), we will recover the expected Gaussian fixed point in high dimensions ($d > 4$) but it becomes unstable when $d < 4$ [4]. We can then obtain the scaling dimension of time as $[t] = \mu^{-4}$. Expanding the noise correlation in Eq. (6c) near the critical point, to leading order we just have Gaussian white noise, so that Eq. (6c) becomes $\mathcal{A}_{\text{noise}} = \int d^d r \int dt (k_B T^{\text{act}} \rho_c / \zeta) \tilde{\varphi} \nabla^2 \tilde{\varphi}$. Therefore, with $[\mathcal{A}_{\text{noise}}] = [\mathcal{A}_0] = \mu^0$ and the first term in Eq. (6b), we conclude:

$$[\varphi(\mathbf{r}, t)] = \mu^{-1+d/2}, \quad [\tilde{\varphi}(\mathbf{r}, t)] = \mu^{1+d/2}. \quad (8)$$

The dimensions of other coefficients in Eq. (6b) can now be straightforwardly determined:

$$\begin{aligned} [g_i] = & \mu^{1+i-(i-1)d/2} (i = 1, 2, \dots), \quad [\kappa_1] = [\kappa_4] = [a] = \mu^0, \\ [\kappa_2] = & [\kappa_3] = [b] = \mu^{1-d/2}, \dots \end{aligned} \quad (9)$$

For $d = 3$, the gradient-expansion terms associated with the coefficients κ_2 , κ_3 , and b are irrelevant in the RG sense,

as their scaling dimensions are negative. This also justifies omitting the higher-order terms in the expansion that were not explicitly considered in Eq. (3). The action near the critical point is thus consistent with the dynamics of Eq. (2) in three dimensions. The presence of the term proportional to g_2 might appear to be consistent with a first-order transition. However, here this is not the case as, at criticality [see Eq. (4)]:

$$g_1 = g_2 = 0. \quad (10)$$

We also note that g_2 term can be formally eliminated by introducing a constant shift in the order parameter:

$$\bar{\varphi}(\mathbf{r}, t) = \varphi(\mathbf{r}, t) - \frac{g_2}{3g_3}. \quad (11)$$

At the critical point, the system is governed by the Wilson-Fisher fixed point, exhibiting behavior characteristic of the Ising universality class. We also note the existence of higher-order \mathbb{Z}_2 violating terms like g_4 in Eq. (5); nevertheless, these terms do not influence the universality class, as established by studies of asymmetric fluid criticality [66–70].

For $d = 2$, the situation is less straightforward since $[\varphi(\mathbf{r}, t)] = \mu^0$, meaning the field is dimensionless. As a result, all coupling terms in Eq. (5) are equally relevant with $[g_i] = \mu^2$. For a scalar order parameter with \mathbb{Z}_2 symmetry, the infinite sequence of coupling terms does not destabilize the Wilson-Fisher fixed point [4]. We can still apply similar arguments as in $d = 3$ to formally eliminate the g_2 term through

a redefinition of φ , and reference the asymmetric fluid literature to demonstrate that higher-order \mathbb{Z}_2 symmetry violating terms do not alter the universality class [66–70]. It may thus appear that the equation of motion [Eq. (2)] continues to yield the Ising universality class in $d = 2$. However, the gradient expansion terms associated with the coefficients κ_2 , κ_3 , and b , as well as the coefficient of $\varphi(\mathbf{r}, t)$ in Eq. (6c), are marginal in the RG sense. Therefore, a more rigorous RG analysis is required to determine whether these terms may destabilize the Wilson-Fisher fixed point in $d = 2$. The analysis will need to consider the non-diagonal terms and multiplicative noise which cannot be immediately discarded in two dimensions.

The marginal terms noted above could perhaps be the source of the contradictory simulation results regarding the universality class for 2D MIPS [24–27]. It was recently suggested that the origins of these conflicting results in $d = 2$ may be the result of additional fixed points identified in AMB+ [30] that coincide with the Wilson-Fisher fixed point for $d \rightarrow 2$ [31]. While the presence of these fixed points have not been established for microscopic models (e.g., ABPs), there is some phenomenology that is superficially consistent with these fixed points, such as microphases [29, 47, 53–55]. Terms which are formally irrelevant in $d = 2 + \epsilon$ might in-

duce a new strong coupling fixed point when $d = 2$, with the Kardar-Parisi-Zhang equation serving as a well-known example [5, 9, 71]. In Ref. [30], the authors employ perturbative dynamical RG techniques at the one-loop level to identify new fixed points in AMB+. These new fixed points coalesce with the Wilson-Fisher fixed point in the limit $d \rightarrow 2$. The authors conjecture one of these new fixed points governs the critical transition from bulk to microphase separation.

Based on our simulation results and approximate coarse-grained dynamics, MIPS should fall within the Ising universality class in $d = 3$, whereas in $d = 2$ our theory is less conclusive. There are currently no reports of microphase separation in 3D particle-based simulations of ABPs, suggesting that the intriguing fixed points of AMB+ are likely absent for ABPs in three dimensions. This is perhaps why both our numerical and theoretical finding appear much more consistent with Ising universality for 3D ABPs in comparison to previous studies in 2D [24–27]. Furthermore, in two dimensions, the dense phase can be a hexatic fluid [53, 72, 73] which introduces an additional order parameter, an effect which may complicate critical scaling analysis and is again absent in three dimensions. Additional theoretical and numerical investigations are needed to pin down the universality class of MIPS in $d = 2$.